Journal of Membrane Science 369 (2011) 20–29

Contents lists available at ScienceDirect

Journal of Membrane Science

journal homepage: www.elsevier.com/locate/memsci

Composite electrolyte membranes for high temperature CO_2 separation

Jennifer L. Wade*, Catherine Lee, Alan C. West, Klaus S. Lackner

School of Engineering and Applied Sciences, Columbia University, New York, NY 10027, USA

ARTICLE INFO

Article history:
Received 6 February 2010
Received in revised form 24 October 2010
Accepted 28 October 2010
Available online 3 November 2010

Keywords:
CO_2 separation
Dual-ion membrane
Carbon capture

ABSTRACT

A membrane device that can selectively separate CO_2 at temperatures exceeding 600 °C has been demonstrated. The membrane can be made from a composite material made of a molten carbonate electrolyte that fills the pore space in a solid oxide electrolyte (e.g. yttria doped zirconia (YSZ), or gadolinia doped ceria (CGO)). The experimental evidence points to a transport mechanism based on opposing ionic currents of carbonate and oxide ions. The flux of CO_2 across these membranes has been shown to increase with temperature, reaching permeabilities of 10^{-11} mol m^{-1} s^{-1} Pa^{-1} (or permeance of 3×10^{-8} mol m^{-2} s^{-1} Pa^{-1}) at 850 °C. The use of a non-ion conducting solid oxide, Al_2O_3, does not result in strong CO_2 permeability or selectivity, supporting a facilitated dual-ion transport mechanism.

1. Introduction

Managing carbon dioxide (CO_2) emissions, by far the largest source of greenhouse gas, is proving to be an ever important technological challenge. Carbon capture and storage, the method of avoiding emissions by separating CO_2 from process gas streams to then permanently store, is relevant in a world where fossil fuel power is still cheap and abundant relative to renewable power generation. High-temperature membrane-based CO_2 separation technology could open the door for innovative process designs ranging from advanced power generation systems, such as IGCC (integrated gasified combined cycle) or novel, carbon fed fuel cells [1]. It is desirable to have a device that can efficiently separate CO_2 at high temperature (>400 °C) and reducing atmospheric conditions.

Membrane systems have the potential to separate CO_2 at lower costs and with lower energy penalties [2,3]. Most CO_2 membrane development is focused on porous polymer and inorganic structures that work best below 200 °C; at higher temperatures the membrane selectivity for CO_2 suffers [3–5]. At elevated temperatures, dense ion conducting membranes can be used for gas separation. Fluorite and perovskite solid oxide structures have been exploited for their fast oxide conduction (O^{2-}) to separate oxygen from a gas mixture, either utilizing a partial pressure gradient or electrical pumping [6]. Similar technologies are being developed for hydrogen separation with high temperature proton conduction [5].

Work on ion conducting membranes for CO_2 separation has built on molten carbonate fuel cell technologies where CO_2 is transported across a molten carbonate electrolyte via electrochemical conversion of O_2 and CO_2 into CO_3^{2-}

$$CO_{2(g)} + 1/2O_{2(g)} + 2e^- = CO_3^{2-} \quad (1)$$

Membranes based on the above reaction require a means of transporting electrons across the membrane, either via electrodes and an external circuit, with or without an applied electromotive force [7,8], or with a composite, mixed conducting material in which transport is driven by oxygen and/or carbon dioxide pressure gradients [9,10]. Such membranes co-transport oxygen and carbonate ions across the membrane and therefore require oxygen in the feed gas. This makes it impossible to separate CO_2 and oxygen and it precludes applications of CO_2 separation from fuel gas mixtures.

In order to separate CO_2 without the concomitant transport of O_2, a dual-ion transport mechanism has been employed [11–15]. Such a mechanism separates CO_2 based on a conversion of CO_2 into CO_3^{2-} with a mixed molten carbonate and solid oxide composite material (Fig. 1). Carbonate and oxide ions are shuttled through the bulk of the membrane in opposing currents.

On the feed side of the membrane, CO_2 combines with an oxide anion, O^{2-}, from the solid oxide phase (so) to form CO_3^{2-}, which then shuttles across the molten carbonate (mc) material, according to the reaction below (2).

$$CO_{2(g)} + O_{(so)}^{2-} = CO_{3\,(mc)}^{2-} \quad (2)$$

On the low CO_2 partial pressure surface, the permeate face of the membrane, the carbonate ion releases CO_2 back into the gas phase, returning the oxide anion to the solid electrolyte, where it travels back to the high partial pressure surface. Unlike the

* Corresponding author. Tel.: +1 646 823 7501.
E-mail address: jlw2103@columbia.edu (J.L. Wade).

0376-7388/$ – see front matter © 2010 Elsevier B.V. All rights reserved.
doi:10.1016/j.memsci.2010.10.053

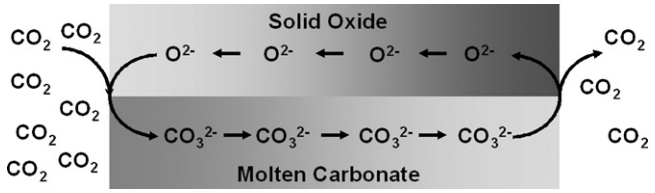

Fig. 1. Schematic depiction of CO_2 transport across a dual-ionic membrane. CO_2 combines with an oxide anion, O^{2-}, to become $CO_3{}^{2-}$. At the opposite surface where the partial pressure of CO_2 is lower, $CO_3{}^{2-}$ ions drop the O^{2-} back into the solid oxide phase, releasing gas phase CO_2. Similar concepts can be located in the literature [11–15].

membranes relying on reaction (1), there is no need for gas-phase oxygen and the short circuited oxide and carbonate currents allow for CO_2 separation in fuel gas mixtures where oxygen partial pressures are negligible. Such a transport mechanism is the basis of the work in this study.

A system where carbonate and oxides are known to interact is between lithium carbonate (Li_2CO_3) and zirconia (ZrO_2). At elevated temperatures (> 650 °C) or low CO_2 pressures, carbonate ions decompose releasing an oxide ion to the zirconia, ZrO_2, forming lithium zirconate (3).

$$Li_2CO_3 + ZrO_2 = Li_2ZrO_3 + CO_2 \quad (3)$$

This process has been shown to be reversible, and Li_2ZrO_3 has been explored as a CO_2 absorbent in the temperature range of 400–650 °C [16–21]. However, the reverse absorption reaction proceeds slowly when the carbonate that forms is in the solid state. In a study by Ida and Lin [18] it was concluded that the kinetics of the absorption reaction is limited by gas phase CO_2 diffusion through the solid carbonate shell. There is an initial rapid uptake of CO_2 onto the zirconate surface until layers of zirconia and lithium carbonate form. At this point CO_2 must diffuse through the solid carbonate layer to reach the zirconia/carbonate interface. If the lithium zirconate is doped with excess alkali–metal carbonates the melting point of the carbonate phase is depressed, resulting in faster CO_2 uptake. The new rate limiting step is dominated by ionic diffusion of O^{2-} and Li^+ through the solid zirconia shell to the reactive interface [18]. Since the original study of lithium zirconate as a CO_2 absorbent material, Nakagawa and Ohashi [16] and other groups have found that sodium zirconate and mixtures made up of lithium, sodium or potassium can provide more effective CO_2 absorption than lithium zirconate alone [22–24].

Membrane structures first making use of the dual-ion conduction mechanism were based on lithium zirconate and related lithium silicate materials [12,13,15]. The lithium zirconate or silicate material absorbed CO_2 from the permeate, splitting into both an oxide conducting and carbonate conducting phase (2). The lithium zirconate based membranes were able to achieve a selectivity of 4.5 for a CO_2/CH_4 mixture and a permeance of $1–2 \times 10^{-8}$ mol m^{-2} s^{-1} Pa^{-1}. The Li_4SiO_4, structure, which is known to absorb CO_2 to form $Li_2SiO_3 + Li_2CO_3$, delivered a total gas permeance of 1×10^{-8} mol m^{-2} s^{-1} Pa^{-1}, and CO_2/N_2 selectivity equal to 5.5 at 550 °C. The flux of CO_2 fell off above 600 °C. The long term performance of these membranes was not reported.

The work presented here differentiates from previous concepts in that a membrane composite is derived from pairs of carbonate and oxide electrolytes optimal for ionic conductivity. This study investigates the chemical reactivity between the phases, which in turn is compared to how these materials behave as dual-phase CO_2 separation membranes. This is different from prior work that began with a reactive zirconate or silicate material that formed subsequent carbonate and oxide phases through CO_2 absorption.

Composite materials made up of doped ceria oxide and carbonate salt, similar to what is being used in this study, is currently being explored as an electrolyte for low temperature solid oxide fuel cells [25–27]. Such a material has shown improved ionic conductivity over electrolytes made from the individual components. It is believed that an enhanced conduction of oxide ions exists at the interface of the two phases [28,29]. Early results have been released showing these same materials can function as CO_2 permeable membranes [14].

In prior work an analytical model was derived to predict the flux of CO_2, J_{CO_2} (mol cm^{-2} s^{-1}) through this dual-ionic system [30]. For purely ionic transport, the carbon dioxide flux can be written as:

$$J_{CO_2} = -\frac{RT}{L_{mem}F^2 4}\left(\frac{\varepsilon\sigma_C(1-\varepsilon)\sigma_V}{\varepsilon\sigma_C + (1-\varepsilon)\sigma_V}\right)\ln\left(\frac{p_{CO_2}(\text{perm})}{p_{CO_2}(\text{feed})}\right) \quad (4)$$

In the above expression, L_{mem} is the membrane thickness, σ_c and σ_v are the conductivities of the $CO_3{}^{2-}$ and vacancy charge carriers (O^{2-} holes), ε is the volume fraction of the carbonate phase, R is the gas constant, F is Faraday's constant, T is absolute temperature, and p_{CO_2} are the partial pressures at the permeate and feed surfaces. Eq. (4) takes on the familiar form of the Wagner equation [31], which is used to describe the flux for mixed ionic-electronic materials limited by bulk ionic transport. The CO_2 flux vanishes in the limit that either conductivity goes to zero. In the carbonate/solid oxide system the oxide conductivity is at least an order of magnitude lower than that of the carbonate phase (≤0.1 S/cm versus ~1.0 S/cm). For alumina the oxide conductivity approaches zero. This flux expression will be compared to the experimental results described within.

2. Materials and methods

2.1. Material characterization

Materials that have high oxygen ion conductivity rates, namely doped zirconia and ceria, were combined with pairs of carbonate mixtures to undergo thermogravimetric testing (TGA) under various atmospheres of CO_2. Any formation of new phases was identified using X-ray diffraction. Finally, the results obtained from the TGA/XRD studies were compared to the isothermal performance of membranes made from these same materials.

2.1.1. Thermogravimetric analysis (TGA)

The precursor materials investigated were lithium, sodium and potassium carbonates (Alfa Aesar, 99.0% purity), 8-mol% yttria doped zirconia (YSZ, Fuel Cell Materials), and 10-mol% gadolinia doped ceria (CGO, Fuel Cell Materials). All powders were dried prior to use in air at 150 °C then combined in a 1:1 stoichiometric ratio by solid state mixing in an agate mortar. The resulting mixture was contained within a shallow platinum pan during testing. Data was collected using a Q50 thermogravimetric analyzer. Gas mixtures of CO_2 and N_2 were combined using integrated mass flow controllers to give total flow rates of 100 mL/min. The CO_2 composition was varied between 10, 50 and 90 mol%. The temperature profile applied in each run was a 4 K min^{-1} heat up to 900 °C with a 3 h hold, followed by a 4 K min^{-1} cool-down to room temperature.

2.1.2. X-ray diffraction (XRD)

The carbonate–oxide mixtures underwent powder X-ray diffraction (XRD) characterization before and after TGA measurements were taken. An Inel X-ray diffractometer with real time detection, CuKα X-ray emission (λ = 1.54 Å) at 30 kV and 30 mA was used. For membrane surface characterization a Scintag Model X2 diffractometer, with CuKα X-ray emission at 45 kV and 30 mA was used. Phase identification was verified with reference data taken from the International Center of Diffraction Data database.

Table 1
Ceramic slurry formulation.

Component		Wet wt%
Ceramic powder + pore former	YSZ + graphite flake	54%
Dispersant	Fish oil	1%
Solvent	Ethyl alcohol	12%
Solvent	Toluene	18%
Binder	Poly(vinyl butyral)	8%
Plasticizer (Type I)	Butylbenzyl phthalate	7%

Table 2
Ceramic sintering profile.

Process step	Control
Heat to 263 °C	1 K/min
Isothermal at 263 °C	60 min
Heat to 738 °C	0.5 K/min
Isothermal at 738 °C	120 min
Heat to 1500 °C	0.5 K/min
Isothermal at final temperature	60 min
Cool to room temperature	1 K/min

Table 3
Composition and melting point of the alkali–metal carbonate mixtures investigated [33].

Carbonate mixture (Li/Na/K – mol%)	Melting point (°C)
100/00/00	**726**
00/100/00	858
00/00/100	899
00/41/59	**710**
43/31/25.0[a]	**397**

[a] Indicates a eutectic mixture.

2.2. Membrane fabrication and characterization

Porous ceramic discs were fabricated from YSZ, CGO or α-alumina (99.95%, Alfa Aesar) using tape casting techniques. The pore structure was created by adding graphite flake (325 mesh, Alfa Aesar) to the tape casting slurry, which acted as a pore forming agent upon burn out in the sintering process. A suspension of the respective oxide powders and the graphite pore formers was made using organic solvents, dispersant, binder and plasticizer that were well mixed in a rotary jar mill with zirconia grinding media. The slurry formulation used in this study is given below in Table 1. The total oxide powder and graphite flake was held constant at 54 wt%.

The suspension was cast into thin films, cut and then sintered in air resulting in 2 cm diameter porous discs with various thickness ranging from 200 to 400 μm. The sintering profile of the ceramics is provided in Table 2. Further details regarding the tape-casting process can be found elsewhere [32]. The porous discs were attached to alumina support tubes using a ceramic sealant (Ceramabond, Aremco). The porosity and pore size distribution were analyzed using mercury porosimetry (Micromeretics Autopore IV) and imaged with a scanning electron microscope (SEM Hitachi 4700).

Once the porous solid oxide ceramic was sealed to an alumina support tube, a measured amount of a carbonate mixture was placed evenly on top of the feed surface of the membrane. Excess carbonate was added to ensure the majority of the pores were filled, including any porous voids in the ceramic seal (e.g. 0.4 g $Li/Na/K_2CO_3 \approx 0.2\ cm^3$ molten volume). The molar ratio of carbonate to oxide was roughly 2:1 in all membrane experiments. The powder melted and filled the pore volume of the solid oxide disk upon heat up within the testing reactor. The alkali carbonates investigated are highlighted in bold in Table 3. The respective melting points of the carbonate mixtures are provided as well.

2.3. Permeation experiments

A schematic of the membrane permeation reactor setup is given in Fig. 2. The membrane and alumina support tube house the permeate stream. An outer Inconel casing seals the alumina support tube from the outside atmosphere and houses the feed stream. The mixed feed stream contains CO_2 and He. The mixture was approximately a 1:1 composition with a total flow rate of 15 mL/min, controlled with Aalborg mass flow controllers (MFC). The admixture was used to determine selectivity and to detect any leaks that may arise in the system, for example, from pinholes or cracks in the membrane or ceramic seal. Heating of the reactor and the gases was controlled with a Tempco Power Console, and all heat up and cool down cycles were carried out at a rate of $2\ K\ min^{-1}$.

The permeate sweep gas was a pre-mixed composition of either argon or helium with 1% CO_2 (certified standard, Praxair) and a total flow rate of 15 mL/min. A small percentage of CO_2 was maintained in the permeate to prevent calcination of the carbonate salts and subsequent volatilization of the oxides (5).

$$\begin{aligned} &M_2CO_{3(1)} = M_2O_{(1)} + CO_2(g) \quad M = Li,\ Na\ or\ K \\ &M_2O_{(1)} = 2M_{(g)} + 1/2O_{2(g)} \end{aligned} \tag{5}$$

The feed and permeate outlets were exhausted to the atmosphere keeping the total pressure of both streams at ambient conditions. Each of the inlets and outlets were sampled with syringes 60 min after the membrane reached temperature to ensure steady state temperature conditions within the reactor. The samples were analyzed using gas chromatography (HP 6850) with a Restek Plot Q column and thermal conductivity detection. The molar flow rate of the gases across the membrane into the permeate stream were derived from mole fraction gas chromatography data, and calculated from a mass balance in the permeate. The molar flow rate of the respective gas species, $\dot{n}_i$ ($mol\ s^{-1}$), is converted to permeability, P ($mol\ m^{-1}\ s^{-1}\ Pa^{-1}$), through the following definition:

$$P_i = \frac{\dot{n}_i}{(p_{i,\text{feed}} - p_{i,\text{permeate}})} \frac{L_{\text{mem}}}{A} \tag{6}$$

where $p_{i,\text{feed}}$ and $p_{i,\text{permeate}}$ are the steady state partial pressures of the gas, i, in the feed and permeate respectively, A is the exposed membrane area, and L_{mem} is the membrane thickness. Note, permeance is an alternative metric reported, and is the permeability divided by the membrane thickness. Selectivity of CO_2 relative to

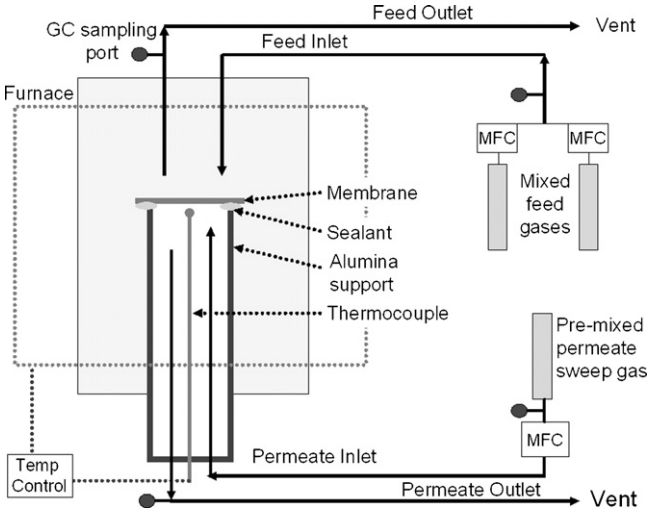

Fig. 2. Schematic of the membrane permeation reactor.

helium, $S_{CO_2,He}$, is defined as the ratio of permeabilities.

$$S_{CO_2,He} = \frac{p_{CO_2}}{p_{He}} \quad (7)$$

3. Analysis and discussion

3.1. Material characterization

3.1.1. YSZ based TGA and XRD

Absolute mass loss over time is given in Fig. 3 for mixtures of YSZ with the carbonate salt combinations shown in Table 3. Each pure carbonate and the two carbonate mixtures were analyzed with TGA separately in order to measure any mass loss due to calcination or volatilization of any decomposition species. Less than 1% of mass loss was seen in these experiments and is not considered to be an important contribution. The same experiment was performed with pure YSZ. YSZ alone resulted in only low temperature mass loss attributed to adsorbed species.

3.1.2. YSZ + Li_2CO_3

Pure lithium carbonate and YSZ showed the greatest mass loss with a rapid decline beginning at 697 °C. Slower mass loss continued over the 3 h dwell at 900 °C. A total of 21 wt% was lost, which corresponds to 99% of the theoretical maximum of CO_3^{2-} releasing CO_2. Upon cooling a slight increase of mass, 0.27 wt%, was observed and this may be attributed to re-absorption of CO_2. X-ray diffraction spectra of the powder mixtures before and after the experiment are given in Fig. 4. They are compared to spectra of pure YSZ powder and crystallized lithium carbonate. The reaction of the two materials up to 900 °C resulted in the formation of lithium zirconate species. Both the monoclinic and tetragonal phases of lithium zirconate were identified (PDF # 01-076-1150 and 00-020-0647, respectively). Further, more yttria rich phases of yttria doped zirconia oxide were identified by the peak shift of YSZ to lower diffraction angles.

The mass loss measured with the Li_2CO_3 + YSZ mixtures is due to the formation of lithium zirconate according to Eq. (3). The formation of lithium zirconate upon the release of CO_2 is an endothermic process that has been shown to proceed above 650 °C [16,18]. Zirconate appeared to form rapidly above 700 °C in our study (Fig. 3). The reverse reaction, where CO_2 is absorbed and measured as mass gain, was not observed during cool-down. The CO_2 absorption reaction becomes spontaneous below 629 °C with the $p_{CO_2} = 0.1$ experimental conditions. In other studies, under an atmosphere of

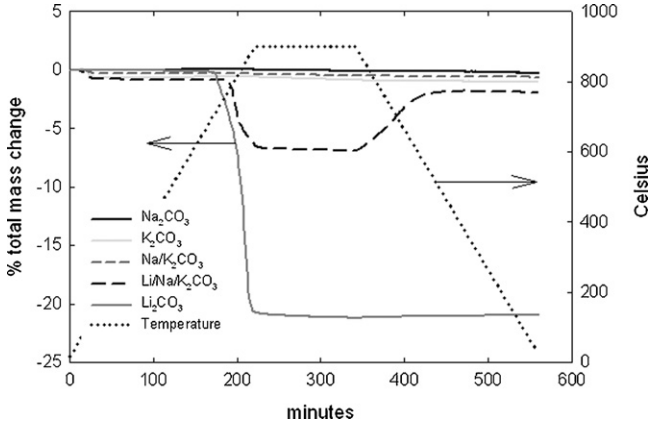

Fig. 3. TGA curves of YSZ and alkali–metal carbonate mixtures in a 10% CO_2 atmosphere (balance N_2, total flow rate = 100 mL min^{-1}). A temperature ramp of 4 K min^{-1} was applied up to 900 °C where the sample was held for 3 h and then ramped down to room temperature.

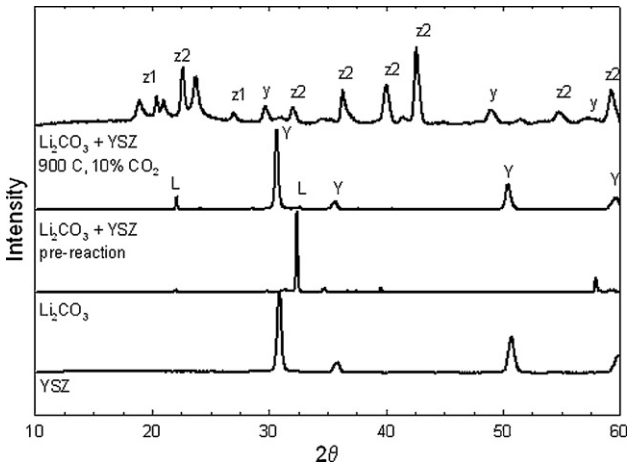

Fig. 4. XRD spectra of both individual Li_2CO_3 and YSZ powders and a 1:1 stoichiometric mixture reacted in 10% CO_2 up to 900 °C. Peak labels correspond as follows: L = Li_2CO_3, Y = cubic YSZ, y = modified cubic YSZ, z1 = monoclinic Li_2ZrO_3 monoclinic phase (PDF # 01-076-1150), z2 = Li_2ZrO_3 tetragonal phase (PDF # 00-020-0647).

CO_2, this reaction has been observed to occur below the melting temperature of pure lithium carbonate, 723 °C [16,17].

It was surprising that no level of CO_2 absorption was measured. A 1:1 mixture of Li_2CO_3 and YSZ was reacted up to 900 °C. The result was a mixture of monoclinic and tetragonal zirconate species and residual YSZ. Both the relatively smaller sized zirconate crystallites (as evidenced by the broader zirconate peaks), and the presence of the faster absorbing tetragonal phase [17] should provide good conditions for CO_2 uptake. Following the double-shell reaction mechanism proposed by Ida and Lin, zirconate absorption of CO_2 should be limited by gas phase CO_2 diffusing through a solid lithium carbonate shell [18]. It was interesting that during cool-down there was never an initial fast uptake of CO_2 that should be able to occur before layers of zirconia and carbonate have established. It is likely the lack of CO_2 uptake was due to the absence of excess molten material at the temperatures where CO_2 uptake should have been observed (<630 °C). In prior powder studies it was noted that excess liquid carbonate was important to get good interfacial contact between dissolved CO_2 and the powdered zirconate phase [17].

3.1.3. YSZ + Li/Na/K_2CO_3

Going back to the TGA mass loss curves in Fig. 3, the tertiary carbonate and YSZ mixture gave rise to mass loss beginning at 765 °C. The maximum mass loss observed (6.8%) corresponds to a 32% conversion of CO_3^{2-} to CO_2. Unlike the pure lithium carbonates, substantial mass was gained with cooling temperature. By the end of the experiment 84% of the original mass loss was recovered. Absorption is possible with tertiary based mixtures because of the lower melting point at 397 °C and due to incomplete reactivity of the carbonate mixture (only a third of the carbonate reacted). This reactive portion may have been due to the 1/3 lithium component in the mix, but this was never directly determined. During cooling the material remains in the molten phase for a longer time, and because the carbonate did not completely react impenetrable shells of tertiary phases, such as zirconate, may not have formed. In short the uptake of CO_2 is not limited to diffusion of the gas molecule through a solid state crystal.

Fig. 5 gives the XRD spectra of the final powder at the end of the TGA experiment compared to the pre-reaction mixture and components.

Two new unidentified peaks were found in the reacted mixture at $2\theta = 28.4°$ and 32.2°. The remaining signals belonged to shifted YSZ peaks and the crystallized tertiary carbonate mixture. The YSZ

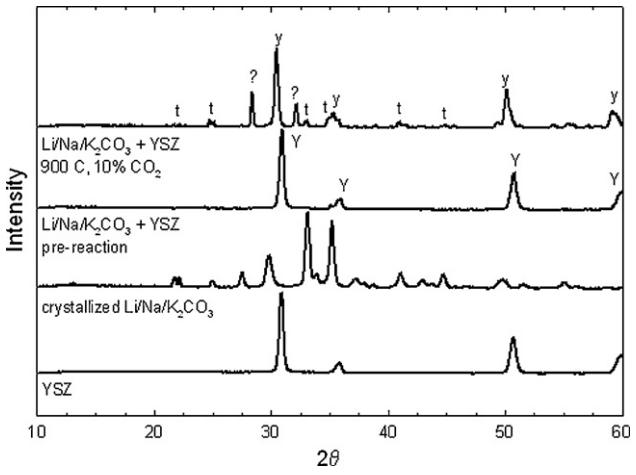

Fig. 5. XRD spectra of crystallized $Li/Na/K_2CO_3$ tertiary carbonate, YSZ powders and a 1:1 stoichiometric mixture reacted in 10% CO_2 up to 900 °C. Peak labels correspond as follows: Y = cubic YSZ, y = modified YSZ, t = crystallized tertiary carbonate mixture, ? = unidentified peaks.

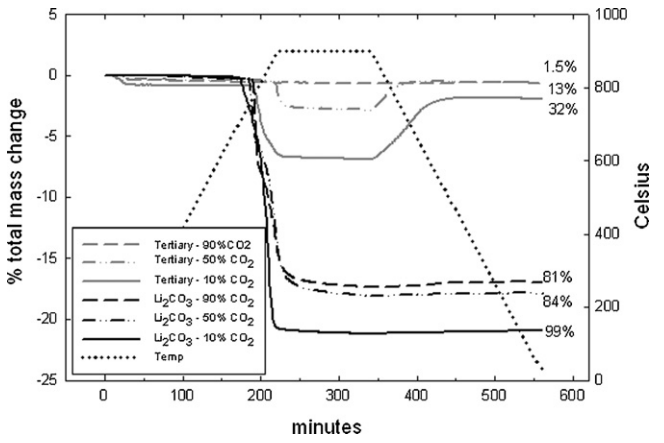

Fig. 6. TGA of tertiary carbonate ($Li/Na/K_2CO_3$) and Li_2CO_3 with YSZ under 10%, 50% and 90% CO_2 atm., balanced with N_2. Percentages indicated the maximum theoretical conversion of CO_3^{2-} to $CO_{2(g)}$. Total flow rate = 100 mL min^{-1}.

and tertiary carbonate is expected if the restored mass returned the materials back into the original phases. Evidence for zirconate formation is not clear with the tertiary salts. The two unidentified peaks may correspond to tertiary phase zirconate material. The carbonate peaks are not evident in the pre-reacted spectra due to their amorphous state.

3.1.4. Na/K_2CO_3

Sodium and potassium carbonate with YSZ mixtures exhibited very little mass loss. All mass loss below 200 °C is assumed to be due to desorption of adsorbed species such as water. Only 0.4% mass loss was measured at higher temperatures. It should be noted that Na_2CO_3 alone was shown to react with YSZ when in the presence of alumina. Understanding the role alumina plays in the formation of sodium zirconate is not within the scope of this paper. However, it is important to note that zirconate formation is possible with sodium carbonate and zirconia, but without the assistance of alumina this reaction is very slow under the CO_2 partial pressure conditions tested in this experiment.

3.2. CO_2 partial pressure dependence

TGA experiments with variable partial pressures in CO_2 emulate the varying conditions that will be imposed upon the membrane surfaces encountered in a separation process. In particular, the two reactive YSZ mixtures (Li_2CO_3 and tertiary carbonate, $Li/Na/K_2CO_3$) were heated under 10, 50 and 90 vol% CO_2 atmospheres. The results of these experiments are given in Fig. 6.

Both carbonate mixtures are dependent on CO_2 partial pressure, with more mass loss occurring in lower CO_2 atmospheres. Further, the onset temperature of mass loss is lower for lower partial pressures of CO_2. The theoretical maximum conversion of the carbonate ions to gas phase CO_2 are shown as percentages next to their respective mass loss curves. These values correspond to the maximum mass loss measured at 900 °C subtracted from the mass at 200 °C. The tertiary mixture did not appear to undergo any reversible mass loss with high CO_2 mixtures ($p_{CO_2} = 0.9$). At 50% CO_2 a theoretical maximum of 13% conversion was achieved and of this mass loss, 98% was recovered. The temperature of the mass loss onset occurred at 884 °C. This is in contrast to the 10% CO_2 run where onset mass loss occurred at 765 °C with a maximum conversion of 32% with 84% mass recovery above 440 °C.

Mass loss measured with lithium carbonate was never recovered under all three partial pressure conditions. However, at higher CO_2 partial pressures less mass loss was measured, and thus a lower conversion of carbonate to gas phase CO_2. The onset temperature of rapid mass loss occurred at 702 °C, 751 °C, and 772 °C, respectively for the 10%, 50% and 90% CO_2 experiments. Thermodynamics tell us that the partial pressure dependence of CO_2 should impact the temperature at which the zirconate reaction proceeds. This is apparent from the Gibb's free energy definition for Eq. (8).

$$\Delta G = \Delta H - T\Delta S + \mathrm{RT}\ln(p_{CO_2}) \quad (8)$$

where ΔH is the positive, endothermic enthalpy change, ΔS is the positive entropy change, R is the gas constant, T is temperature and p_{CO_2} is the partial pressure of CO_2. Thus, the higher the partial pressure, the higher the temperature necessary before the zirconate reaction can become spontaneous. Under the three CO_2 partial pressures investigated, spontaneous lithium zirconate formation can occur at 629 °C, 727 °C and 771 °C, respectively. From the experiments above it shows that temperatures in excess of 700 °C were necessary to kinetically allow the lithium zirconate reaction to proceed. Again, this time with higher partial pressures of CO_2, the zirconate phase was unable to absorb CO_2.

Exact thermodynamic data of the tertiary phase materials are not available but the trends are the same, whereby CO_2 release requires higher temperatures under higher CO_2 partial pressure atmospheres (Fig. 6). Likewise, the reverse CO_2 absorption reaction can proceed at higher temperatures. It is interesting to see that the tertiary mixture will not undergo a decarbonation reaction when exposed to high partial pressures of CO_2 and temperatures below 900 °C.

3.3. CGO + carbonates

Mass loss curves were obtained for 1:1 stoichiometric mixtures of CGO, a known oxide conductor, and alkali–metal carbonates (Fig. 7). All the experiments exhibited a similar mass loss profile, including the experiment with CGO alone. The percent total mass loss for the CGO alone, 5.82%, was greater than the others (with the exception of K_2CO_3 + CGO). This mass loss occurred only in a single run, a second heating profile of the same material did not result in greater than 1% mass loss. Further, pure CGO was examined in 100% N_2 and 10%O_2 atmospheres but this data is not presented in the figure.

The run of CGO in 10% O_2 resulted in 0.7% less mass loss than in the 100% N_2 and 10% CO_2 experiment. From this it is assumed that the majority of the mass loss observed with the CGO powders can be attributed to adsorbed species likely present from the processing of the submicron starting powders. There is an additional smaller

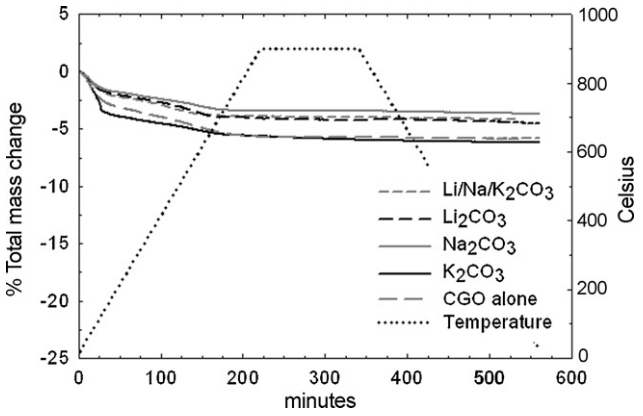

Fig. 7. TGA experiments of alkali–metal carbonate and 10-mol% gadolinia doped ceria (CGO) mixtures under 10% CO_2 atmospheres, balance N_2. Total flow rate = 100 mL min^{-1}.

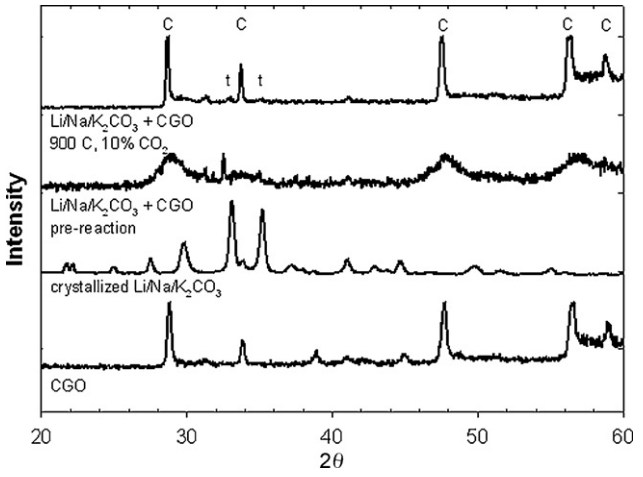

Fig. 8. XRD spectra of crystallized Li/Na/K_2CO_3 tertiary carbonate, CGO powders and a 1:1 stoichiometric mixture reacted in 10% CO_2 up to 900 °C. Peak labels correspond as follows: C = 10% gadolinia doped ceria, t = crystallized tertiary carbonate mixture.

contribution to mass loss that is due to the removal of oxygen from the ceria crystal lattice. This is known to occur in ceria, which can accommodate extra oxygen vacancies due to the reduction of Ce^{4+} cations to Ce^{3+} cations [34]. The extra mass loss in the K_2CO_3 mixture (over that of the other mixed carbonate/ceria experiments) occurred below 140 °C. The potassium carbonate salts are deliquescent, and if contaminated with bicarbonate ions will release water and carbon dioxide above 120 °C to form the carbonate species [35].

The XRD analysis of the mixtures before and after TGA heat cycles is provided in Fig. 8. Only the respective crystallized carbonates and CGO peaks are identified. There is no evidence for the formation of a new crystalline phase with the CGO based mixtures, and it is believed that no significant chemistry between the two materials occurred under the conditions of the TGA experiment. This is in agreement with other work that has explored these materials for low temperature electrolytes in solid oxide fuel cells [27,36]. Because CGO is a known oxide conductor, and is unique in that it does not appear to chemically react with the carbonate salts, it is of interest to test the performance of this electrolyte in a membrane system in order to see if CO_2 separation is possible in the absence of zirconate chemistry.

3.4. Membrane characterization

SEM images of room temperature porous YSZ membrane cross sections before and after infiltration with a molten carbonate salt are provide in Fig. 9. The pore size distributions of pre- and post-infiltration for the YSZ, CGO and Al_2O_3 membrane structures is given in Fig. 10a–c.

In the SEM image in Fig. 9a, the dominant pore diameter of the porous YSZ was around a micron, and this was confirmed with the mercury porosimetry measurements provided in Fig. 10a, showing pore diameters ranging from 0.2 to 3 μm. The total pore volume within the oxide phase was 34% prior to infiltration. Fig. 10b and c give the pore size distributions for the CGO and Al_2O_3 based membranes. The total porosity of these membranes is similar, 36% and 38%, but the pore size range is tighter. Given the high surface tension of molten alkali carbonate salts ($\gamma \sim 200$ mN/m) [33], and the excellent wetability on oxide surfaces (i.e. contact angle, $\theta = 0$), capillary forces are sufficient to retain the molten salt in the pore space. Using the Young–Laplace equation for cylindrical pores, (Eq. (9)) relating capillary force to the pressure differential across the pore, ΔP, a pressure of 0.4 MPa can be applied for 1 μm sized pores before blowout will occur.

$$\Delta P = \frac{2 \times \gamma \times \cos\theta}{R} \tag{9}$$

Both the post-infiltration image (Fig. 9b) and mercury porosimetry data (Fig. 10a–c) demonstrate the filling of the pore volume by the carbonate phase. The predominate micron sized pores were eliminated from infiltration, and only sub-micron pores remained after cooling. The total pore volume was reduced to 6% or lower. Any remaining void volume measured for the infiltrated membrane could be due to the contraction of the molten carbonate upon cooling ($\rho_{molten,750\,°C} = 1.96\,g\,cm^{-3}$ versus $\rho_{molten,25\,°C} = 2.54\,g\,cm^{-3}$)[33]. Based on this difference in density, up to 7.5% porosity at room temperature can be possible, in good agreement with the measured 6% porosity. Sealing of the pores by the tertiary molten carbonate was complete at 500 °C, and was noted by a sharp decrease in helium measured in the feed.

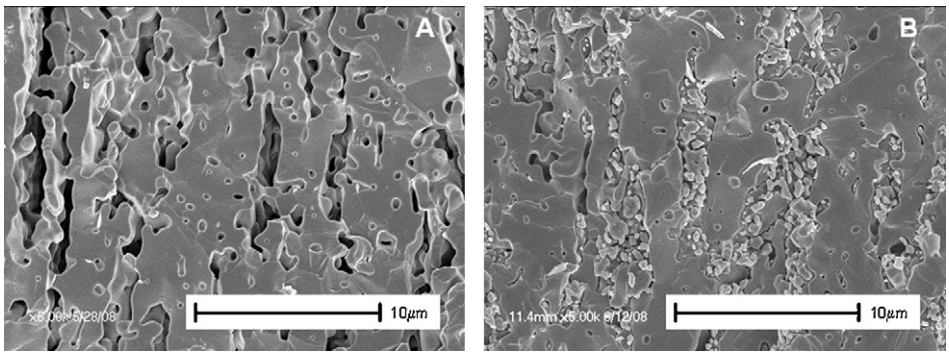

Fig. 9. SEM images of membrane cross sections: (a) un-infiltrated YSZ and (b) tertiary salt infiltrated YSZ. Infiltrated image taken after carbonate salt was frozen.

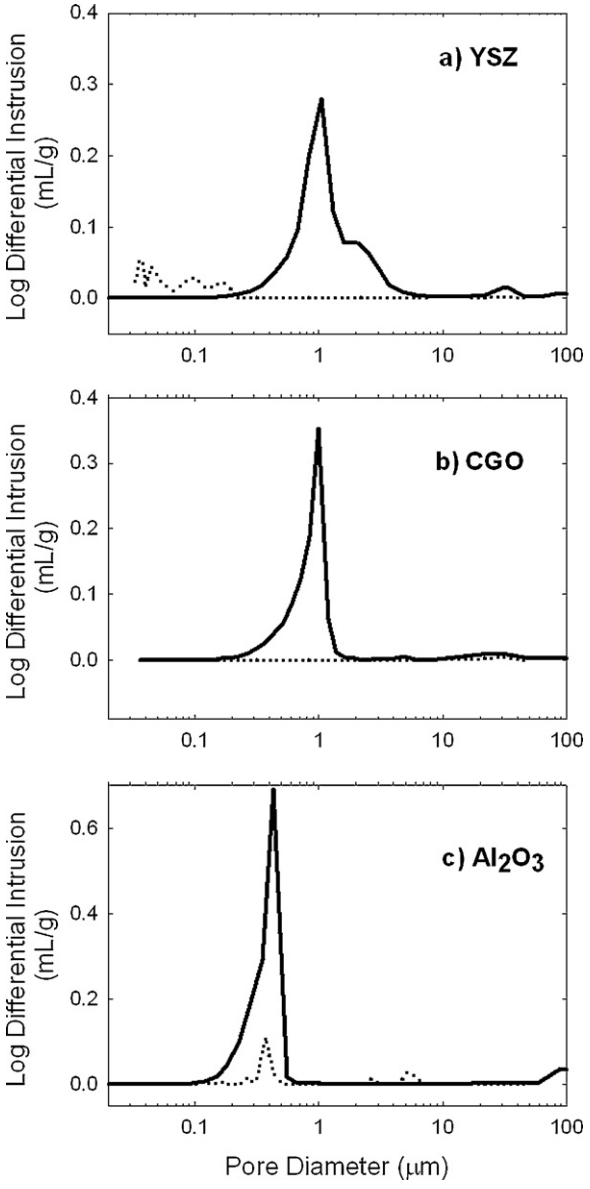

Fig. 10. (a–c) Pore-size distribution of pre- (dotted) and post- (solid) infiltrated (a) YSZ, (b) CGO, and (c) Al_2O_3 membranes with corresponding total pore volumes of the room temperature membranes.

3.5. Membrane CO_2 permeability

3.5.1. Membrane sealing

To ensure membrane sealing by the molten salt infiltrating the oxide pore space, a null experiment was completed with a membrane made from a YSZ/tertiary carbonate composite. Helium was provided in the feed chamber and the resulting permeability into the permeate stream was monitored upon heating the membrane to 800 °C (Fig. 11). The concentration of CO_2 was maintained at 1 vol% in both the feed and permeate stream to minimize calcination effects. In Fig. 11 the He permeability is as high as 2×10^{-10} mol m^{-1} s^{-1} Pa^{-1} at 300 °C. By 400 °C, just above the melting point of the tertiary eutectic salt (397 °C), the He permeability falls three orders of magnitude to 10^{-13} mol m^{-1} s^{-1} Pa^{-1}, indicating the filling of the pores and sealing of the membrane.

3.5.2. Isothermal experiments

Membranes made up of porous YSZ were infiltrated with mixtures of pure Li_2CO_3, Li/Na/K_2CO_3 eutectic and Na/K_2CO_3 mixture.

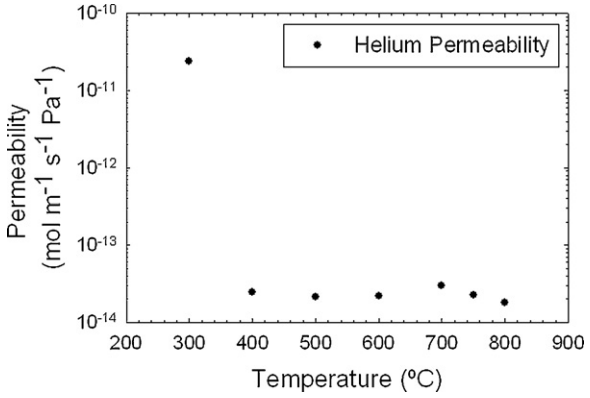

Fig. 11. Helium permeability of aYSZ/carbonate membrane upon heating in the permeation reactor. P_{He} feed = 0.99 atm.

Porous CGO and α-Al_2O_3 ceramics infiltrated with the tertiary carbonate eutectic were investigated as well. These particular carbonate mixtures were chosen because they all had melting points below 750 °C (Table 3). The membranes were all tested at 750 °C, and the CO_2 permeability across the membranes over time is shown in Fig. 12.

Both helium and CO_2 were present in the feed stream as a 1:1 mixture, and helium permeability never exceeded 5×10^{-13} mol m^{-1} s^{-1} Pa^{-1} (experiments are terminated if He leaking is measured above 1×10^{-12} mol m^{-1} s^{-1} Pa^{-1}). In the absence of any facilitated transport mechanism that favors CO_2 permeance, helium has been shown to leak at approximately twice the rate of CO_2. Permeability of helium is caused by leaking through pores in the seal connecting the membrane to the support tube and from any unfilled pores within the membrane structure itself. To correct the CO_2 flux for any contribution due to leaking half of the helium permeability is subtracted from that of CO_2.

$$P^* = P_{CO_2} - 1/2P_{He}$$

The use of a non-oxide conducting membrane, α-Al_2O_3, was used as a control experiment against the oxide conducting YSZ and CGO based membranes. The objective was to examine the relevance of oxide ion conductivity to the transport mechanism. Alumina is an insulating material that has virtually zero oxide conductivity, and therefore should result in very low bulk CO_2 permeability relative to the YSZ and CGO based membranes. This experiment was sustained beyond 4000 minutes and over this duration CO_2 permeability never exceeded 8×10^{-13} mol m^{-1} s^{-1} Pa^{-1}. Unlike the ceria and zirconia based porous oxide membranes, the low CO_2 perme-

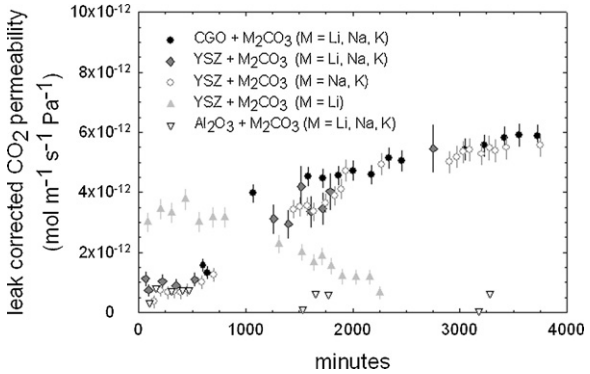

Fig. 12. CO_2 permeability at 750 °C with composite membranes made up of CGO + Li/Na/K_2CO_3, YSZ with Li_2CO_3, Li/Na/K_2CO_3, and Na/K_2CO_3 and Al_2O_3 Li/Na/K_2CO_3 mixtures. Membrane thickness ranged from 200 to 400 μm.

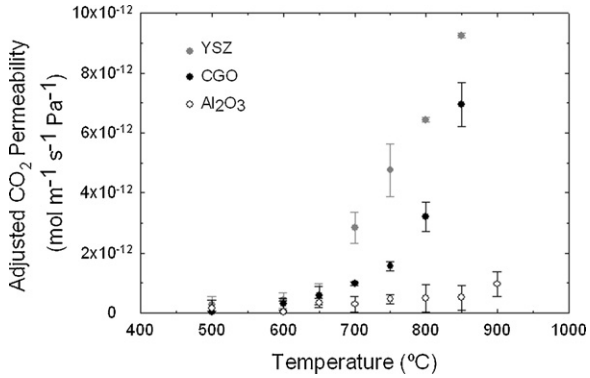

Fig. 13. Average CO_2 permeability with YSZ, CGO and Al_2O_3 based membranes with molten tertiary carbonate eutectic. Half of the helium permeability is subtracted from that of the CO_2 to adjust for contributions due to leaking. Error bars corresponds to 1σ deviations over 2–3 separate experiments. Membrane thickness ranged from 200 to 400 μm.

ance with the non-oxide conducting alumina membrane did not support a flux of CO_2.

With the YSZ based membranes the lithium carbonate behaved differently from that of the binary and tertiary mixtures. With the pure lithium carbonate salts, the membrane performance was initially between 3 and 4×10^{-12} mol m^{-1} s^{-1} Pa^{-1}. The performance gradually dropped to below 1×10^{-12} mol m^{-1} s^{-1} Pa^{-1} after 37 h and less than 8 h later the membrane began to leak. Two additional experiments were repeated with YSZ and Li_2CO_3, and each showed the same trend of permeability decay and membrane failure below 36 h. Membrane failure was determined by the background helium permeability, noted by orders of magnitude increase in He permeability, 10^{-13} up to 10^{-11} mol m^{-1} s^{-1} Pa^{-1}.

It is believed that the pure lithium carbonate based membrane failed due to the formation of a zirconate phase, which has shown to occur with the previous TGA data. Zirconate formation results in a 34% volume expansion of the zirconia lattice [16]. Because this expansion will not occur uniformly across the structure, it is not difficult to imagine the creation of compressive stresses that can lead to membrane cracking. Further, the formation of a zirconate phase may create new porous voids. Early in the experiment the void spaces can be immediately filled in with excess molten liquid carbonate. Once a critical amount of the carbonate has converted, a fraction of the pores may be left unfilled leading to membrane leaking.

The membranes made up of the tertiary ($Li/Na/K_2CO_3$) and the binary (Na/K_2CO_3) carbonate mixture with YSZ showed similar permeability trends, however, in opposition to what was observed with the pure lithium carbonate. The CO_2 permeability began relatively low, around 1×10^{-12} mol m^{-1} s^{-1} Pa^{-1}, and then increased to $5–6 \times 10^{-12}$ mol m^{-1} s^{-1} Pa^{-1} over 2500 min. Upon reaching the higher permeability levels shown in Fig. 13, the membranes appeared to reach a steady state with lifetimes extending past 10,000 min in one run. Comparing the tertiary carbonate YSZ based membranes to those of the Li/YSZ it is clear that the former is more stable. Looking back at the TGA data of tertiary carbonate and YSZ materials, the formation of secondary phase (possibly a zirconate phase) is easily reversible and not all of the carbonate is converted. These effects may explain the higher permeability measured over longer periods of time relative to the membranes with pure lithium carbonate. The Na/K mixture was examined in membrane permeability experiments because there was no apparent reactivity with YSZ powder based on TGA (Fig. 3) and XRD data. However, similar permeabilities were achieved with these membranes as with the Li/Na/K carbonate based membranes. The permeability was initially low over the first 500 min and then increased to over 5×10^{-12} mol m^{-1} s^{-1} Pa^{-1} during the next 2000 min. This is evidence that the CO_2 separation mechanism is independent of the formation of a third phase.

The avoidance of zirconate chemistry altogether was tested by examining the non-reactive oxide material, CGO. The tertiary carbonate mixture and CGO membranes resulted in strong and increasing permeability, similar to that of the YSZ experiments with the tertiary or sodium/potassium carbonate mixtures. The time-dependent permeability of CO_2 was similar to that of the YSZ based experiment, beginning between 1 and 2×10^{-12} mol m^{-1} s^{-1} Pa^{-1} and increasing over time to values between 5 and 6×10^{-12} mol m^{-1} s^{-1} Pa^{-1}. The permeability appeared to have stabilized within this region and continued for over 120 h. It is clear with CGO/carbonate material that a dual-ion conducting mechanism can occur without the formation of an additional phase. The explanation of the time dependence of these membranes is currently unclear.

3.6. CO_2 permeability and temperature dependence

CO_2 permeability as a function of temperature with tertiary carbonate/oxide based membranes is given in Fig. 13. Each data point is an average over 2–3 replicate experiments. The measurements were taken 60 minutes after reaching steady state temperatures.

CO_2 permeability in the YSZ and CGO based membranes was shown to increase with temperature. Averaged permeability at 850 °C reached 7.0×10^{-12} mol m^{-1} s^{-1} Pa^{-1} ± 11% (or permeance of 2.3×10^{-8} mol m^{-2} s^{-1} Pa^{-1}). With Al_2O_3 based membranes, CO_2 permeability did not show a strong increase with temperature. In these runs the selectivity of CO_2/He remained between 0.4 and 0.5 until 800 °C at which point CO_2 became slightly selective over He, ($S_{CO_2,He}$ = 1–2 within 800 °C and 900 °C). However, the CO_2 permeability measured at 800 °C and 900 °C is lower than the average YSZ and CGO permeabilities at 800 °C. This lack of permeability with alumina (also seen in Fig. 12) supports the necessity of an oxide conducting material to complete the CO_2 transport mechanism.

CO_2 permeability data for the YSZ and CGO based membranes are compared in Fig. 14 to the analytical transport model derived for the bulk, dual-ionic transport mechanism. By converting the CO_2 flux equation (Eq. (4)) to permeability, membrane porosity and temperature dependent oxide and carbonate conductivities can be inputted for comparison to experimental data. Table 4 lists the extrapolated temperature dependent conductivities for the carbonate and vacancy species (σ_c and σ_v), ceramic pore volume, ε, and CO_2 feed pressures used in the respective experiments [33,34].

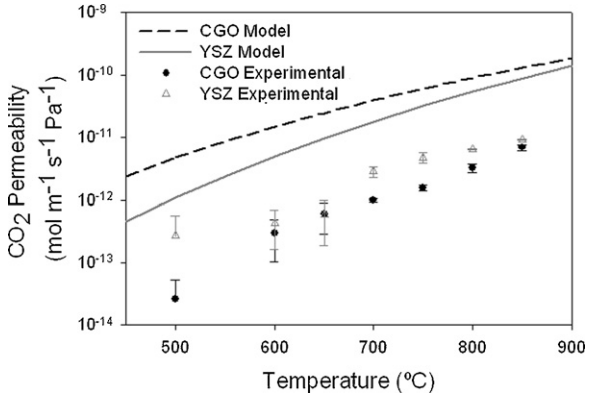

Fig. 14. Average CO_2 permeability with CGO and YSZ based membranes with molten tertiary carbonate. CO_2 permeability based on the ionic transport model is given for the same materials. Calculations are based on Eq. (4).

Table 4
Model parameters input into Eq. (4).

Temp (°C)	σ_c (S cm^{-1}) [24]	σ_v (S cm^{-1}) [27] (YSZ)	σ_v (S cm^{-1}) [27] (CGO)
400	0.3	0.0002	0.002
500	0.7	0.001	0.006
600	1.2	0.005	0.017
700	1.8	0.015	0.040
800	2.6	0.043	0.086
900	3.5	0.106	0.167

	YSZ	CGO
ε	0.34	0.39
P_{CO_2}(feed), Pa	44,000	51,700

Comparing the experimental data to the dual-ionic model, a 1–2 order of magnitude discrepancy exists. The explanation for the lower than expected flux rates is currently unclear. However, above 600 °C the slope of the experimental data agrees well with the model. This is evident by calculating the activation energy of the averaged conductivity. YSZ activation energies were 84 ± 14 kJ mol^{-1} versus 81 kJ mol^{-1} predicted with literature values input into the analytical expression (Eq. (4)). CGO activation energies were 77 ± 6 kJ mol^{-1} versus 59 kJ mol^{-1} predicted with literature values. The similarity in the observed temperature activation suggests that the dominating resistance is controlled by the conductivity of the solid oxide phase. Based on the known higher conductivity of CGO oxides at lower temperatures, particularly with composite CGO and carbonates, this material is expected to outperform YSZ. Yet, at this time the uncertainty introduced in the measurements by the temporal effects precludes a detailed analysis. Several phenomena can explain the lower than expected permeabilities and work is currently underway to better understand what these are. One explanation for the higher permeability with YSZ based membranes may be due to the zirconate chemistry occurring at the carbonate/oxide interface. Further, surface kinetic constraints, composite conductivities and tortuosity of the two phases are all possible effects impacting the transport of these membranes.

4. Conclusions

High temperature membranes based on dual carbonate and oxide electrolytes have been shown to selectively separate CO_2 above 600 °C in the absence of gas phase oxygen. Pairs of alkali–metal carbonates and two solid oxide conductors, YSZ and CGO, were examined using thermogravimetric analysis and X-ray diffraction. These results were compared with the isothermal performance (750 °C) of membranes made up of pairs of the same electrolyte materials. The YSZ based membranes and lithium carbonate react irreversibly to form lithium zirconate. These materials, when used as membranes, function well initially but the permeability declines with time. This is believed to be due to the formation of a zirconate phase interfering with the CO_2 transport mechanism. Tertiary carbonates made up of lithium, sodium and potassium have been shown to react reversibly with YSZ, and membranes made up of these materials reach CO_2 permeabilities of 5×10^{-12} mol m^{-1} s^{-1} Pa^{-1} (or CO_2 permeance of 2.0×10^{-8} mol m^{-2} s^{-1} Pa^{-1}) at 750 °C. The YSZ based membranes composed only of sodium and potassium carbonates function similarly despite their slow reactivity with zirconia. CGO based membranes do not show any sign of chemical reactivity with the alkali carbonates based on the TGA and XRD results, yet membranes infiltrated with tertiary carbonates selectively permeate CO_2, reaching permeabilities of 6×10^{-12} mol m^{-1} s^{-1} Pa^{-1} (or CO_2 permeance of 3×10^{-8} mol m^{-2} s^{-1} Pa^{-1}). When using a non-oxide conducting, alumina based membrane, very low CO_2 permeability was measured.

The successful performance of a non-zirconia oxide based membrane proves that the CO_2 transport mechanism functions in the absence of zirconate chemistry and opens the door for a wide range of other oxide materials to be explored for the purpose of selective CO_2 permeability at high temperatures. Further, the lack of permeability in the absence of oxide conductivity supports that the CO_2 transport results from the interplay between carbonate transport in the molten carbonate and oxide ion transport in the solid oxide phase. It is not a stretch to imagine analogous devices for separation of other gas species, (e.g. sulfides, ammonia) based on similar dual-ion transport mechanisms. The demonstration and future refinement of a new type of membrane that has near perfect separation opens the door for advanced process technology involving high temperature gas separation.

Acknowledgements

Funding for this work was provided by the Energy Innovations Small Grant program under the California Public Interest in Energy Research foundation, contract no. 060232. TGA and XRD data collection was made possible with Columbia University's NSF MRSEC Shared Instrument Facility.

Nomenclature

A	membrane active area, cm or m
CGO	10-mol% gadolinia doped ceria
D_i	diffusion coefficient of species i, cm^2 s^{-1}
G	Gibbs free energy, kJ mol^{-1}
F	Faraday's constant, 96,485 C/mol equiv.
H	enthalpy, kJ mol^{-1}
J_i	flux of species i, mol cm^{-2} s^{-1}
L_{mem}	membrane thickness, cm or m
L_{film}	molten carbonate film thickness, cm
$\dot{n}_i$	molar flow rate, mol s^{-1}
p_i(feed)	partial pressure of species i in feed, atm.
p_i(permeate)	partial pressure of species i in permeate, atm.
P_i	permeability of species i, mol m^{-1} s^{-1} Pa^{-1}
P_i^*	leak corrected permeability, mol m^{-1} s^{-1} Pa^{-1}
R	ideal gas constant, 8.314 J K^{-1} mol^{-1}
S	entropy, J K^{-1} mol^{-1}
$S_{i,j}$	selectivity of species i over species j
T	temperature, K
YSZ	8-mol% yttria stabilized zirconia
Z_C	charge of carbonate = −2
Z_V	charge of vacancies = +2

Greek symbols

ε	volume fraction of molten carbonate (i.e. solid oxide porosity)
σ_i	conductivity, S cm^{-1}

Subscripts and superscripts

C	carbonate ion
g	gas phase
l	liquid phase
MC	molten carbonate phase
SO	solid oxide phase
S	solid phase
V	oxide vacancy

References

[1] J. Wade, K. Lackner, Development of a Coal-based Solid-Oxide Fuel Cell System in the 30th International Technical Conference on Coal Utilization & Fuel Systems, Clearwater, FL, 2005.

[2] M. Mulder, Basic Principles of Membrane Technology, Kluwer Academic Publishers, Dordrecht, 1991, p. 363.

[3] D. Shekhawat, D.R. Luebke, H.W. Pennline, A Review of Carbon Dioxide Selective Membranes, Department of Energy, National Energy Technology Laboratory, 2003.

[4] E.J. Granite, T. O'Brien, Review of novel methods for carbon dioxide separation from flue and fuel gases, Fuel Processing Technology 86 (2005) 1423–1434.

[5] R. Bredesen, K. Jordal, O. Bolland, High-temperature membranes in power generation with CO_2 capture, Chemical Engineering and Processing 43 (2004) 1129–1158.

[6] Y. Teraoka, T. Nobunaga, K. Okamoto, N. Miura, N. Yamazoe, Influence of constituent metal cations in substituted $LaCoO_3$ on mixed conductivity and oxygen permeability, Solid State Ionics 48 (1991) 207–212.

[7] J.L. Weaver, J. Winnick, The molten carbonate carbon dioxide concentrator: cathode performance at high CO_2 utilization, Journal of the Electrochemical Society 130 (1983) 20–28.

[8] T.H. Etsell, S.N. Flengas, The electrical properties of solid oxide electrolytes, Chemical Reviews 70 (1969) 340–378.

[9] S.J. Chung, J.H. Park, D. Li, J.I. Ida, I. Kumakiri, J.Y.S. Lin, Dual-phase metal–carbonate membrane for high temperature carbon dioxide separation, Industrial & Engineering Chemistry Research 44 (2005) 7999–8006.

[10] A.F. Sammells, Mixed conducting membrane for carbon dioxide separation and partial oxidation reactions, in: USPTO, Eltron Research, Inc., United States, 2004, p. 31.

[11] K.S. Lackner, A.C. West, J.L. Wade, Membrane for carbon dioxide separation at high temperatures, in: WO2006113674, U. Columbia, Editor, United States, 2006.

[12] H. Kawamura, T. Yamaguchi, B.N. Nair, K. Nakagawa, S.-i. Nakao, Dual-ion conducting lithium zirconate-based membranes for high temperature CO_2 separation, Journal of Chemical Engineering of Japan 38 (2005) 322–328.

[13] Y. Li, Z. Rui, C. Xia, M. Anderson, Y.S. Lin, Performance of ionic-conducting ceramic/carbonate composite material as solid oxide fuel cell electrolyte and CO_2 permeation membrane, Catalysis Today 148 (2009) 303–309.

[14] T. Yamaguchi, T. Niitsuma, B.N. Nair, K. Nakagawa, Lithium silicate based membranes for high temperature CO_2 separation, Journal of Membrane Science 294 (2007) 16–21.

[15] M. Anderson, Y.S. Lin, Carbonate–ceramic dual-phase membrane for carbon dioxide separation, Journal of Membrane Science 357 (2010) 122–129.

[16] M. Anderson, Y.S. Lin, Synthesis and Characterization of Carbonate–Ceramic Dual-Phase Membranes for Carbon Dioxide Separation, in: R. Bredesen, H. Rader (Eds.), Proceedings of the 9th International Conference on Inorganic Membranes, 2006, pp. 678–681.

[17] K. Nakagawa, T. Ohashi, A novel method of CO_2 capture from high temperature gases, Journal of the Electrochemical Society 145 (4) (1998) 1344–1346.

[18] B.N. Nair, T. Yamaguchi, H. Kawamura, S.-I. Nakao, Processing of lithium zirconate for applications in carbon dioxide separation: structure and properties of powders, Journal of the American Ceramic Society 87 (2004) 68–74.

[19] J.-I. Ida, Y.S. Lin, Mechanism of high temperature CO_2 sorption on lithium zirconate, Environmental Science Technology 37 (2003) 1999–2004.

[20] R. Xiong, J. Ida, Y.S. Lin, Kinetics of carbon dioxide sorption on potassium-doped lithium zirconate, Chemical Engineering Science 58 (2003) 4377–4385.

[21] K.N. Essaki, Kazuaki, K. Masahiro, Acceleration effect of ternary carbonate on CO_2 absorption rate in lithium zirconate powder, Journal of the Ceramic Society of Japan 109 (2001) 829–833.

[22] D.J. Fauth, E.A. Frommell, J.S. Hoffman, R.P. Reasbeck, H.W. Pennline, Eutectic salt promoted lithium zirconate: novel high temperature sorbent for CO_2 capture, Fuel Processing Technology 86 (2005) 1503–1521.

[23] A. Lopez-Ortiz, N.G.P. Riviera, A.R. Rojas, D. Lardizabal, Novel carbon dioxide solid acceptors using sodium containing oxides, Separation Science and Technology 39 (2004) 3359–3572.

[24] H. Pfeiffer, C. Vazquez, V.H. Lara, P. Bosch, Thermal behavior and CO_2 absorption of $Li_{2-x}Na_xZrO_3$ solid solutions, Chemistry of Materials 19 (2007) 922–926.

[25] M.Y. Veliz-Enriquez, G. Gonzalez, H. Pfeiffer, Synthesis and CO_2 capture evaluation of $Li_{2-x}K_xZrO_3$ solid solutions and crystal structures of a new lithium-potassium zirconate phase, Journal of Solid State Chemistry 180 (2007) 2485–2492.

[26] B. Zhu, X.G. Liu, P. Zhou, X.T. Yang, Z.G. Zhu, W. Zhu, Innovative solid carbonate-ceria composite electrolyte fuel cells, Electrochemistry Communications 3 (2001) 566–571.

[27] J. Huang, Z. Mao, Z. Liu, C. Wang, Development of novel low-temperature SOFCs with co-ionic conducting SDC-carbonate composite electrolytes, Electrochemistry Communications 9 (2007) 2601–2605.

[28] C. Xia, Y. Li, Y. Tian, Q. Liu, Y. Zhao, L. Jia, Y. Li, A high performance composite ionic conducting electrolyte for intermediate temperature fuel cell and evidence for ternary ionic conduction, Journal of Power Sources 188 (2009) 156–162.

[29] B. Zhu, S. Li, B.E. Mellander, Theoretical approach on ceria-based two-phase electrolytes for low temperature (300–600 degrees C) solid oxide fuel cells, Electrochemistry Communications 10 (2008) 302–305.

[30] W. Zhu, C.R. Xia, D. Ding, X.Y. Shi, G.Y. Meng, Electrical properties of ceria-carbonate composite electrolytes, Materials Research Bulletin 41 (2006) 2057–2064.

[31] J.L. Wade, K.L. Lackner, A.C. West, Transport model for a high temperature, mixed conducting CO_2 separation membrane, Solid State Ionics 178 (2007) 1530–1540.

[32] I. Riess, Electrochemistry of mixed ionic-electronic conductors, in: P.J. Gellings, H.J.M. Bouwmeester (Eds.), The CRC Handbook of Solid State Electrochemistry, CRC Press, Boca Raton, FL, 1997, pp. 223–268.

[33] J.L. Wade, High Temperature Carbon Dioxide Separation Membrane, Department of Chemical Engineering, Columbia University, New York City, 2008, pp. 145.

[34] J.R. Selman, H.C. Maru, Physical chemistry and electrochemistry of alkali carbonate melts: with special reference to the molten-carbonate fuel cell, in: G. Mamantov, J. Braunstein, C.B. Mamantov (Eds.), Advances in Molten Salt Chemistry, Plenum Press, New York, 1981, pp. 159–389.